CORA Cork Open Research Archive
Cartlann Taighde Oscailte Chorcaí

Title	Intra-annual variability in the performance of an oscillating water column wave energy converter
Authors	López, I.;Carballo, R.;Iglesias, Gregorio
Publication date	2020-02-03
Original Citation	López, I., Carballo, R. and Iglesias, G. (2020) 'Intra-annual variability in the performance of an oscillating water column wave energy converter', Energy Conversion and Management, 207, 112536 (10pp). https://doi.org/10.1016/j.enconman.2020.112536
Type of publication	Article (peer-reviewed)
Link to publisher's version	10.1016/j.enconman.2020.112536
Rights	© 2020, Elsevier Ltd. All rights reserved. This manuscript version is made available under the CC BY-NC-ND 4.0 license. - https://creativecommons.org/licenses/by-nc-nd/4.0/
Download date	2026-11-16 11:30:59
Item downloaded from	https://hdl.handle.net/10468/9836

UCC
University College Cork, Ireland
Coláiste na hOllscoile Corcaigh

Intra-annual variability in the performance of an oscillating water column wave energy converter

I. López[a,*], R. Carballo[a], G. Iglesias[b,c]

[a] *Univ. de Santiago de Compostela, Área de Ingeniería Hidráulica, EPSE, Campus Universitario s/n, 27002, Lugo, Spain.*
[b] *MaREI, Environmental Research Institute & School of Engineering, University College Cork, College Road, Cork, Ireland.*
[c] *University of Plymouth, School of Engineering, Marine Building, Drake Circus, Plymouth, PL4 8AA, United Kingdom.*

Abstract

The intra-annual variability in the wave resource is often disregarded when analysing the performance of wave energy converters (WECs), despite the fact that this variability is substantial in the majority of the areas of interest for the development of wave energy. The objective of this work is to analyse and quantify the intra-annual variability in the performance of oscillating water column (OWC) WECs through a case study in Galicia (NW Spain). To this end a three-step methodology which combines numerical and experimental modelling is followed: (i) intra-annual wave energy resource matrices are determined numerically through a high-resolution procedure; (ii) efficiency matrices of the device are determined by means of physical modelling, considering the influence of air compressibility and different turbine specifications represented through different values of turbine-induced damping; and (iii) finally, intra-annual energy capture matrices are calculated by combining the resource and efficiency matrices. It is found that the intra-annual variability in the energy capture of an OWC converter is significant, over 20% in the case study considered, albeit slightly smaller than that of the wave energy resource itself. The turbine-induced damping exerts a modulating effect over the variability in the intra-annual captured energy. Furthermore, the optimum damping which maximises the performance of the OWC converter varies from month to month.

Keywords

Oscillating water column; physical modelling; air compressibility; numerical modelling; wave energy; turbine-induced damping

* Corresponding author
e-mail address: ivan.lopez@usc.es (I. López)

Nomenclature

Roman symbols

A_c	Area of the chamber in plan view [m^2]
B^*	Dimensionless damping coefficient [–]
C_g	Wave group velocity [m s^{-1}]
C_{WR}	Capture-with ratio [–]
D	Diameter of the orifice that simulates the turbine [m]
E_p	Total pneumatic energy per unit width of converter [MWh m^{-1}]
E_w	Total wave energy per metre of wave front [MWh m^{-1}]
H_{m0}	Significant wave height [m]
P_p	Pneumatic power captured by the device [W]
P_w	Wave power per metre of wave front [W m^{-1}]
Q	Flow rate [$m^3 s^{-1}$]
S	Spectral wave energy density [$m^2 Hz^{-1} rad^{-1}$]
T_e	Wave energy period [s]
V_m	Air volume of the OWC chamber at model scale [m^3]
V_p	Air volume of the OWC chamber at prototype [m^3]
g	Gravitational acceleration [m s^{-2}]
h	Water depth [m]
k	Wave number [m^{-1}]
n_p	polytropic exponent of the turbine [–]
t_{max}	Total time of the tests [s]
w	Width of the OWC converter [m]

Greek symbols

Δp	Pressure drop [Pa]
δ	Tank-to-sea water density ratio [–]
θ_{mean}	Mean wave direction [º]
λ	Linear scale factor [–]
ρ_a	Air density [kg m^{-3}]
ρ_w	Water density [kg m^{-3}]
ω	Wave angular frequency [rad s^{-1}]

Acronyms

EMEC	European Marine Energy Centre
BBDB	Backward Bent Duct Buoy
JONSWAP	Joint North Sea Wave Observation Project
OWC	Oscillating water column
RANS	Reynolds-averaged Navier–Stokes equations
VOF	Volume of fluid
WEC	Wave energy converter
iWEDGE	Intra-annual wave energy diagram generator

1. Introduction

Wave energy is one of the most promising energy sources under development, thanks to four fundamental characteristics. First, the worldwide wave energy resource is vast and, importantly, widely available [1,2]. Second, it can be exploited without a high impact [3]. Third, it is easily predictable [4,5]. Last, but not least, its exploitation allows synergies with other marine renewables to be realised [6,7]. On the downside, the wave energy resource presents significant variability on different timescales, from decadal to seasonal to individual waves, which poses challenges for the design and exploitation of efficient and robust wave energy converters (WECs).

Over the last few years, numerous works have been carried out to analyse the variability in the wave energy resource, considering both inter-annual [8] and intra-annual timescales [9,10]. In particular, it has been shown that the locations with the largest amount of wave energy present a great intra-annual variability in the available resource [11]. This variability goes beyond a mere seasonality, and monthly variations have been shown to significantly affect the performance of WECs [12,13]. It follows that an intra-annual characterisation of the wave energy resource is the first step towards a comprehensive evaluation of the performance of a given WEC at a site of interest. Although the variability in the captured energy is typically smaller than the variability of the wave energy resource itself, it remains very significant; indeed, monthly differences in the range of 156%-384% have been found depending on the WEC technology [12].

Among the wide variety of WECs developed over the last decades, including oscillating water column (OWC) devices [14], oscillating body systems [15] and overtopping converters [16], OWC devices are one of the most successful. They consist of a partially submerged empty chamber open to the sea below the free surface, and an air turbine. Wave action excites the water column inside the chamber, which oscillates vertically, forcing the air above to alternately flow into and out of the chamber, and in the process driving the turbine. Unless a rectifying system with non-return valves is provided, a special turbine design, capable of operating under bidirectional flow, is required. Wells (reaction) and impulse (action) turbines are typically used [17]. The simplicity of the system—only a chamber and an air turbine—and its suitability for being integrated into coastal structures [18,19], with the consequent benefit regarding the reduction of construction costs, are some of the main advantages of OWC converters.

When evaluating the energy production of an OWC device at a given coastal site, which implies the analysis of the performance of the converter under a wide range of sea states (irregular waves), the

most common solution is to make use of theoretical hydrodynamic models, both frequency-domain and time-domain models. Among them, frequency-domain models are probably the most employed. Although there are many examples in the recent literature, only a few are focused on evaluating the energy production in a real case study. A frequency-domain stochastic model was developed in [20] to calculate the annual power performance of the OWC plant on Pico Island (Portugal), equipped with a Wells turbine. On this basis, a method for optimising the turbine size of the Pico OWC was proposed in [21]; two alternative criteria were followed: maximum energy production and maximum economical profit. The stochastic method was also used for optimising the annual power extracted by a floating-type OWC converter operating in the western coast of Portugal [22]. More recently, a frequency-domain hydro-thermodynamic model was proposed by [23] in order to evaluate the annual energy production of a Backward Bent Duct Buoy (BBDB) floating OWC device for the wave conditions off the west coast of Ireland. However, although frequency-domain models are computationally undemanding, they present the disadvantage of being limited to linear problems, i.e., those involving small amplitude waves and linear turbines (e.g., Wells).

On the other hand, time-domain models allow the consideration of non-linear effects as well as the analysis of non-linear turbines (e.g., impulse turbines). A time-domain model for a BBDB device off the west coast of Vancouver Island (Canada) was presented in [24]; the model includes some non-linear effects namely: mooring forces, viscous drag and air compressibility, which were found of great importance for adequately modelling the converter. The performance of the OWC plant at the breakwater of Mutriku (Spain) was also investigated through time-domain models. First, in [25] the annual average performances of two air turbines, a Wells turbine and a biradial turbine [26], were compared. Second, in [27] the influence on the power production performance of the plant of three speed control strategies for the biradial turbine was analysed. Finally, a time-domain model was developed in [28] for evaluating the annual power performance of the Tupperwave floating OWC device and compared to that of a conventional floating OWC, both located at the European Marine Energy Centre (EMEC) wave energy test site, off the coast of Scotland.

When a most accurate analysis is needed, two alternatives emerge: (i) computational fluid dynamic (CFD) models based on the Reynolds-averaged Navier–Stokes (RANS) equations, and (ii) physical models. RANS models, with the help of a turbulence closure model, determine the velocity fields on the entire domain, being capable of solving the non-linear wave-converter interactions, including complex phenomena such as wave breaking. Moreover, by using the volume of fluid (VOF)

technique [29], these models manage to accurately capture the air-water interface. A RANS-VOF numerical model was applied to study the annual energy capture of an OWC plant at the breakwater of A Guarda (Spain) in [30]. Similarly, the annual performance of a breakwater-integrated OWC converter on the southern Brazilian coast was evaluated through a RANS-VOF model [31]. Regarding physical model tests, they are still one of the best options in order to obtain trustworthy results, avoiding numerical approximations and uncertainties and high computational times. Physical modelling was used for evaluating the annual energy capture of an OWC device at three different locations in the north west coast of Spain [32].

Despite the great number of models presented above for evaluating the energy production of an OWC device at a given coastal site, all of them analyse the energy production of the device in annual average figures. Taking into account the fact that the performance of an OWC depends on both the wave conditions and the turbine-induced damping [33], and considering that the variability in the wave conditions is typically large in the areas of interest for wave energy exploitation, the intra-annual variability in the performance of an OWC and its relationship with the turbine-induced damping must be investigated—and therein lies the motivation and novelty of the present work.

The methodology followed in the present piece of research combines numerical and physical modelling. First, the intra-annual wave energy resource characterisation matrices at a location of interest—for illustration, a case study in NW Spain was considered—were computed through high-resolution spectral numerical modelling based on the energy bin concept. Second, the efficiency matrices of the OWC wave energy converter were determined by means of physical modelling—therefore, considering non-linear effects—taking into account specifically the influence of air compressibility and considering three (non-linear) impulse turbines of different characteristics, emulated through three values of the turbine-induced damping, an essential parameter to be considered when studying OWC devices [34,35]. Lastly, the intra-annual energy capture matrices (one per each turbine-induced damping) were computed by combining the intra-annual resource matrices with the efficiency matrices of the device. The paper is organized as follows. In Section 2, the location and main characteristics of the study site are presented. The methodology is described in Section 3, and the results of its application to the case study are described and discussed in Section 4. Finally, the main conclusions are summarised in Section 5.

2. Study site

The installation of an OWC in Corme, a medium-size port in Galicia (NW Spain), was considered for the study (Figure 1). Corme is in the coastal stretch known as the Death Coast, extending from Cape Finisterre to the Sisargas Isles. The entrance of the port is located at a depth of approx. 12 m at mid tide. This area stands out for its vast wave energy resource [36], which is subject to a very significant intra-annual variability [9]. For these reasons Corme is well suited as a case study for this research.

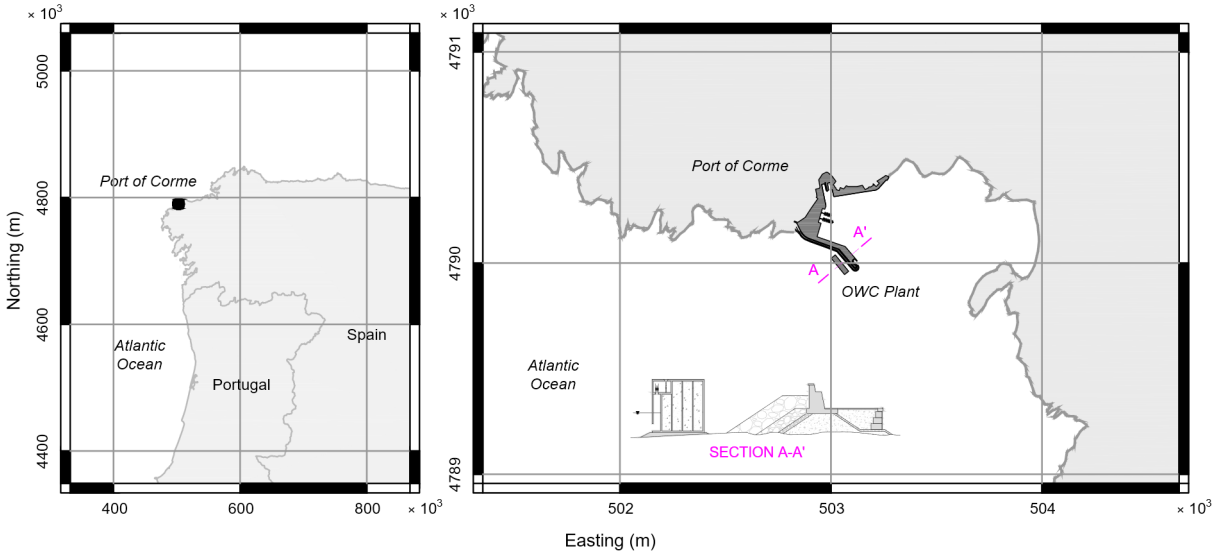


Figure 1. Location of the study site, the Port of Corme, with a sketch of the proposed OWC device (coordinate reference system ETRS89 - UTM zone 29N).

3. Materials and methods

3.1. Numerical model

As established in Section 1, an appropriate analysis of the intra-annual variability in the performance of an OWC at location of interest should be conducted based on a thorough knowledge of the existing wave conditions at this specific site. The information required for this analysis should consist of characterization matrices with the same level of resolution as that of the efficiency matrix of the OWC and covering time periods short enough in order to appropriately characterise the intra-annual variation of the wave resource, which in turn may well lead to significant intra-annual variations in the performance of the OWC considered.

With this in view, the methodology iWEDGE (intrannual Wave Energy Diagram Generator) [9,12] is used in order to obtain the required information at the selected location. The methodology is based on the energy bin concept, or energy intervals describing the available energy and occurrence of combinations of the relevant wave spectral parameters. The implementation of this procedure is

179 divided in three main steps. First, the deepwater wave energy resource in the area of interest is
180 characterized by analysing deepwater in situ data recorded by the Silleiro's deepwater buoy, being the
181 result a 3D characterization matrix providing the distribution of the total energy available along with
182 its intra-annual occurrence amongst trivariate energy bins, i.e., energy bins whose intervals are
183 defined by combinations of significant wave height (H_{m0}), energy period (T_e), and mean wave
184 direction (θ_{mean}). In the second step, the most energetic bins providing 95% of the total wave energy
185 resource are propagated towards the coastal location of interest by means of high-resolution spectral
186 numerical modelling. Finally, the resulting wave conditions of H_{m0} and T_e for all the energy bins
187 propagated are obtained at the grid node closest to the selected location. This information together
188 with the intra-annual occurrence of each selected bin is used to reconstruct 2D characterization
189 matrices composed of bivariate energy bins (or energy intervals of H_{m0} and T_e), i.e., the required
190 information for conducting accurate intra-annual performance analysis [12,37].

191 3.2. Physical model

192 The experimental campaign was performed in the wave flume of the University of Santiago de
193 Compostela. The tests were carried out at a 1:25 scale. The experimental set-up and the geometry of
194 the model are depicted in Figure 2. Nine wave gauges located along the flume and two ultrasonic level
195 sensors located in the interior of the chamber were set to monitor the free surface elevations and the
196 oscillations of the water column. Moreover, a differential pressure sensor was allocated to monitor the
197 relative pressure inside the chamber.

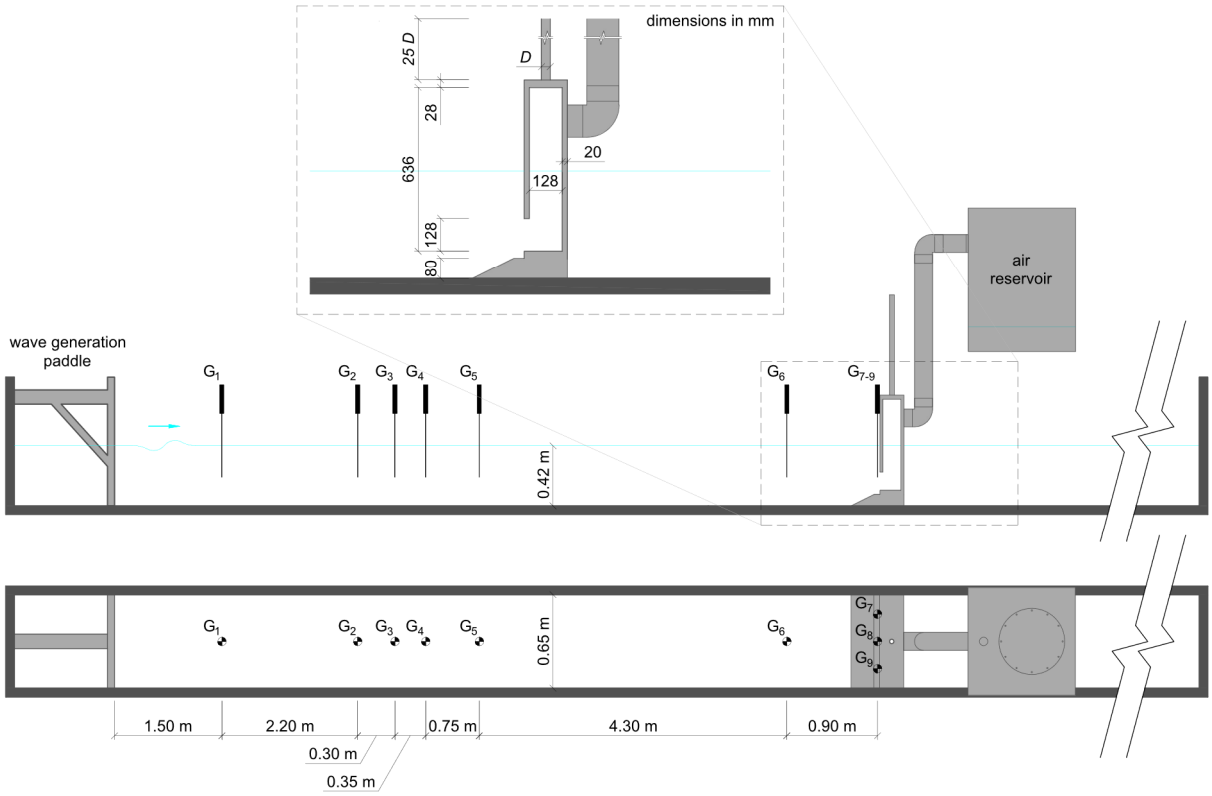


Figure 2. Side and plan view of the experimental set-up.

The OWC model follows, in its submerged part, the Froude similitude criterion—*sine qua non* condition when free-surface flows are involved [38]—and full geometrical similarity. However, for correctly modelling air compressibility effects, which are essential to avoid significant errors in the evaluation of the performance of an OWC device [39,40], the air volume in the chamber (V) must be scaled according to [41]:

$$\frac{V_p}{V_m} = \lambda^2 n_p \delta \ , \tag{1}$$

where the subscripts p and m indicate prototype and model, respectively; λ is the linear scale factor; n_p is the polytropic exponent of the turbine; and δ is the water density ratio. Thus, a distorted aerial part was set to accomplish a total air volume in the chamber of, according to Eq.(1), V_m = 538.4 dm^3. As shows Figure 2, the extra air volume was achieved by connecting an air reservoir to the OWC model chamber [41].

Amongst the two most common OWC turbines (Wells and impulse), the self-rectifying impulse turbines were chosen in this work due to the fact that its average efficiency is kept practically unchanged within a wide range of sea states and, in addition, they present a lower level of noise in comparison with Wells turbines [17], which is an important feature for port-located OWC devices.

Impulse turbines present a quadratic pressure-vs-flowrate relation [42]. Therefore, the turbine-induced damping was modelled through orifices of different diameter [43,44]. Unlike with Wells turbines, with self-rectifying impulse turbines the turbine-induced damping barely depends on the rotational speed of the turbine [14], and therefore a turbine of a given diameter can be simulated through a single orifice for the complete range of operating conditions. The orifices were characterised by means of the damping coefficient, defined as

$$B^* = \frac{\Delta p^{1/2}}{Q} \frac{A_c}{\rho_a^{1/2}} \,, \tag{2}$$

where Δp is the pressure drop between the interior of the chamber and the atmosphere; Q is the flow rate through the orifice; A_c is the area of the chamber in plan view; and ρ_a is the density of air. The ratio $\Delta p^{1/2} Q^{-1}$ was obtained following López *et al.* [32]. A summary of the different parameters that characterise the orifices is presented in Table 1.

Table 1. Diameter (D), opening ratio (ratio between the area of the orifice and the plan area of the chamber), pressure-vs-flowrate relation ($\Delta p^{1/2} Q^{-1}$) and damping coefficient (B^*) for the different orifice diameters tested.

***D* (mm)**	***Opening ratio* (%)**	**$\Delta p^{1/2} Q^{-1}$ (kgm^{-7})**	***B**** **(–)**
39	1.5	1.48×10^6	84.85
31	1.0	3.59×10^6	132.18
28	0.8	5.30×10^6	160.49

The testing programme comprised forty-nine irregular wave conditions, resulting from the combination of five significant wave heights, (H_{m0} = 0.79, 1.65, 2.60, 3.57 and 4.55 m) and eleven energy periods (T_e = 4.5, 5.5, 6.5, 7.5, 8.5, 9.5, 10.5, 11.5, 12.5, 13.5 and 14.5 s). These wave conditions, generated following a JONSWAP-type spectra [45], are representative of an equal number of energy bins (Figure 3).

The efficiency of the OWC device under each wave condition was evaluated based on the capture-width ratio, defined as:

$$C_{WR} = \frac{P_p}{P_w w} \,, \tag{3}$$

where w is the width of the device (dimension orthogonal to the incident wave direction); P_p is the pneumatic power captured by the device, calculated following

$$P_p = \frac{1}{t_{max}} \int_0^{t_{max}} \Delta p(t) Q(t) dt \,, \tag{4}$$

where t_{max} is the total time of the test.

Finally, P_w is the incident wave power per metre of wave front, defined as:

$$P_w = \rho_w g \int_0^\infty S(\omega) C_g(\omega) d\omega \ , \tag{5}$$

where ρ_w is the water density; g is the gravitational acceleration; $S(\omega)$ is the spectral density of the incident wave; and C_g is the group velocity defined as

$$C_g(\omega) = \frac{1}{2}\frac{\omega_i}{k_i}\left(1 + \frac{2k_i h}{\sinh 2k_i h}\right), \tag{6}$$

where ω_i and k_i are the angular frequency and the wave number of each ith frequency band; and h is the water depth. The wave number is related to the angular frequency through the dispersion relation:

$$\omega_i^2 = g k_i \tanh k_i h \ . \tag{7}$$

The efficiency of all the sea states included within the intervals of an energy bin is assumed to be the same, being all of them characterised by the most representative wave condition previously selected. Therefore, the capture-width ratios of the forty-nine wave conditions define, for each value of the damping coefficient, the efficiency matrices of the OWC (Figure 3). A comprehensive description of the experimental tests can be found in [32].

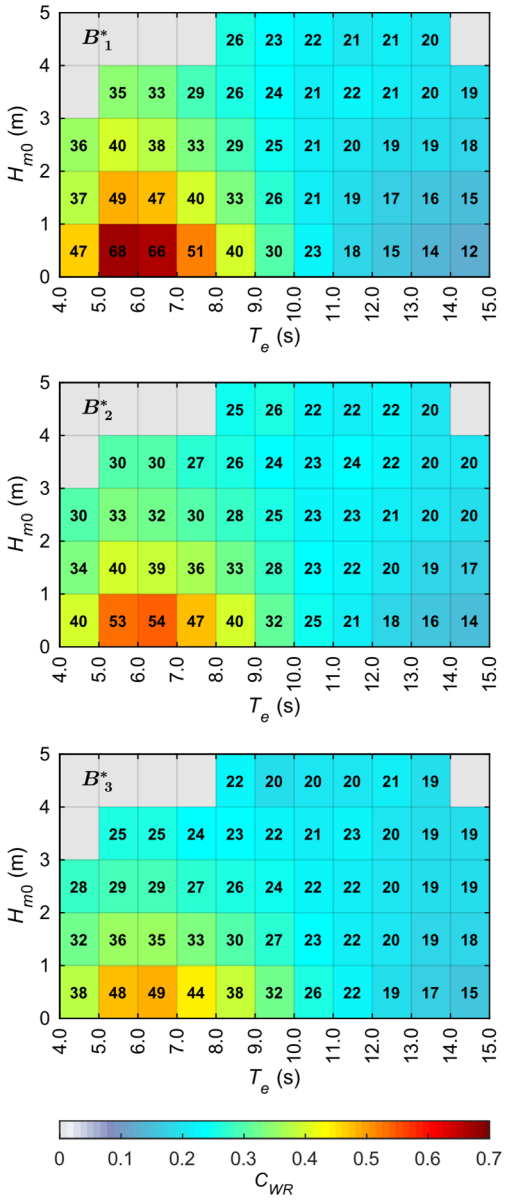


Figure 3. OWC efficiency matrices expressed in term of the capture-width ratio (C_{WR}) for the three values of the turbine-induced damping tested (B^*_1 = 84.85; B^*_2 = 132.18; B^*_3 = 160.49).

4. Results and discussion

4.1. Intra-annual wave resource

The intra-annual wave resource characterisation matrices corresponding to the location of interest are presented for the months of January, April, July and October (Figure 4) with a view to covering the four seasons. A great intra-annual variability in the wave energy resource can be clearly observed. Among the represented months, January is the one that presents the largest amount of wave energy, as shown by the more reddish colours (more wave energy available) of its energy bins. In this month, the bulk of energy is provided by sea states with significant wave heights between 1 and 3 m, and energy

periods between 9 and 10 s. In addition, the wave energy resource is distributed over a wide range of wave heights up to 4 m. In October, although the wave energy is distributed again over sea states with wave height up to 4 m, the wave energy provided is lower than in January (yellowish colours of the energy bins). The largest amount of energy is provided by sea states with significant wave heights between 1 and 2 m, and energy periods between 8 and 9 s. The wave energy is even lower in April. In this month, the bulk of energy is provided by sea states of similar characteristics to those in October (1 m < H_{m0} < 2 m and 8 s < T_e < 9 s). The wave energy resource, however, is distributed over a comparatively narrower range of wave heights (0 m < H_{m0} < 3 m). Finally, July is the month with the lowest wave energy of the four analysed. The resource is distributed in the narrowest range of wave heights of all the months (0 m < H_{m0} < 2 m), and the bulk of energy is provided by energy bins in the range 0 m < H_{m0} < 1 m and 6 s < T_e < 7 s.

In sum, the wave energy resource distribution varies along the year going from a typical winter situation (e.g., January) in which the largest amount of energy is provided by sea states with energy periods between 9 and 10 s and significant wave heights between 1 and 2 m, to a typical summer situation (e.g., July) in which the largest amount of energy is provided by sea states with energy periods between 6 and 7 s and significant wave heights between 0 and 1 m, with an intermediate situation in the remaining months (e.g., April and October). That is, the bulk of energy moves towards lower energy periods and wave heights during summer months.

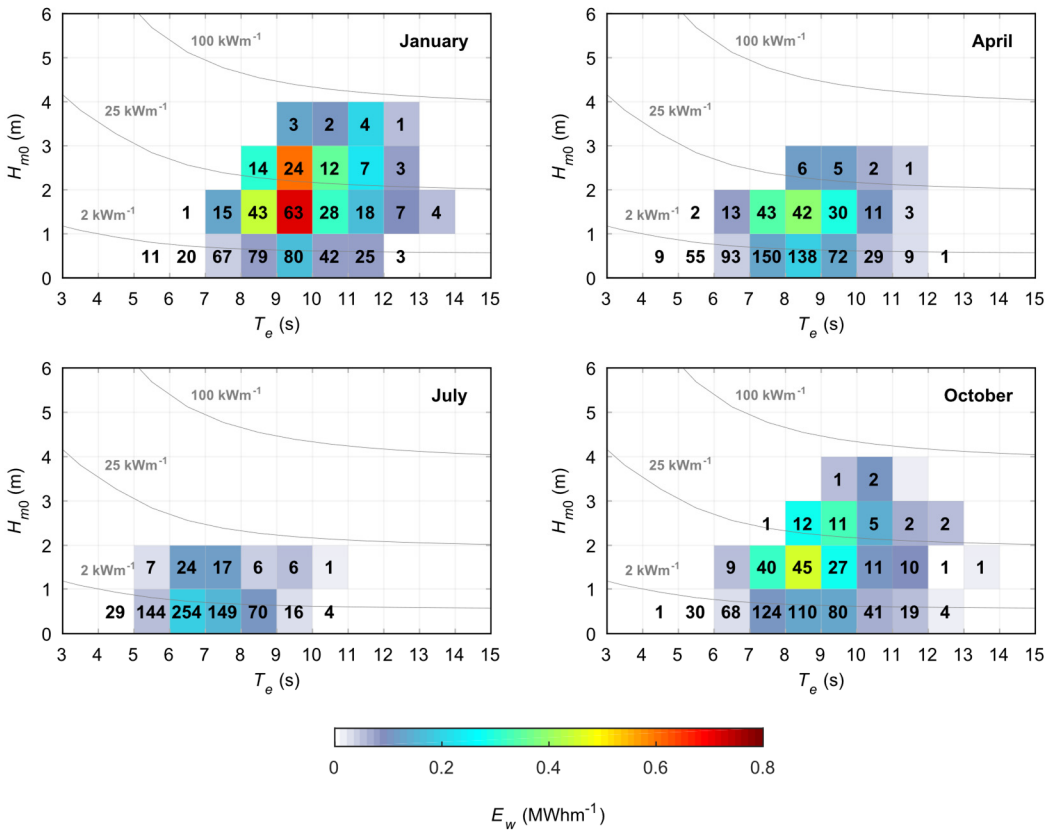


Figure 4. Intra-annual wave resource characterisation matrices for four different months. The colour scale indicates the total energy per metre of wave front (E_w) supplied by each energy bin and the numbers inside the bins provide the occurrence, in hours, of the sea states within each bin. The wave power is indicated by the isolines.

To better comprehend the intra-annual variability of the wave energy resource, the available wave energy is represented on a monthly basis in Figure 5. A great variability in the intra-annual available energy can be clearly observed, in accord with previous studies in the region [9]. It was found that between the least and the most energetic months ($E_{w,\,aug}$ = 0.8 MWhm^{-1} and $E_{w,\,jan}$ = 4.5 MWhm^{-1}, respectively) there is an increase of the available energy of more than 400%. From the total annual available wave energy ($E_{w,\,annual}$ = 27.1 MWhm^{-1}), the months of January ($E_{w,\,jan}$ = 4.5 MWhm^{-1}) and February ($E_{w,\,feb}$ = 4.1 MWhm^{-1}), that constitute only 16.2% of the time in a year, provide 31.7% of the total available resource. The opposed situation takes place in the period from May to September that, despite constituting 41.9% of the time in a year, provide only 22.2% of the total annual available energy. These strong monthly variations in the available energy emphasise the importance of an intra-annual analysis of high temporal resolution (e.g., monthly).

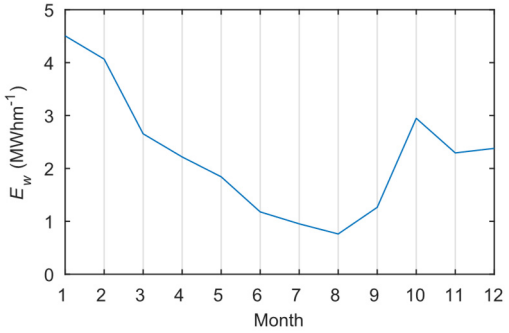


Figure 5. Intra-annual wave energy resource in an average year.

4.2. Intra-annual variability in the OWC performance

The combination of the OWC efficiency matrices (Figure 3) with the intra-annual resource matrices (Figure 4) is presented in Figure 6 for the months of January, April, July and October. The great influence of the wave energy resource on the captured energy is apparent; in fact, the energy bins that provide the bulk of captured energy match those providing the largest amount of available energy for the three values of the damping. For example, in January the energy bin which supplies the largest amount of captured energy is delimited, for the three values of the turbine-induced damping, by energy periods between 9 and 10 s and significant wave heights between 1 and 2 m, corresponding to the energy bin contributing the most to the available energy resource in that month (Figure 4). An analogous situation takes place in July and October. Interestingly, in April the turbine-induced damping presents a comparatively higher influence, i.e., the energy bin which supplies the largest amount of captured energy changes depending on the value of the damping coefficient. Thus, for the highest damping (B^*_3) the energy bin that supplies the largest amount of captured energy is bounded by 8 s < T_e < 9 s and 1 m < H_{m0} < 2 m; for the lowest damping (B^*_1) it is bounded by 7 s < T_e < 8 s and 1 m < H_{m0} < 2 m; finally, for the intermediate damping (B^*_2), the two aforementioned energy bins provide virtually the same captured energy. In any case, even in those months in which the energy bin that supplies the largest amount of captured energy does not change with the turbine-induced damping, the influence of this factor on the captured energy is unequivocally high. For example, in July, paying attention to the energy bin that supplies the largest amount of captured energy, the highest damping coefficient provides 26% less captured energy ($E_{p,\,jul}$ = 0.10 MWhm^{-1}) than the lowest one ($E_{p,\,jul}$ = 0.13 MWhm^{-1}).

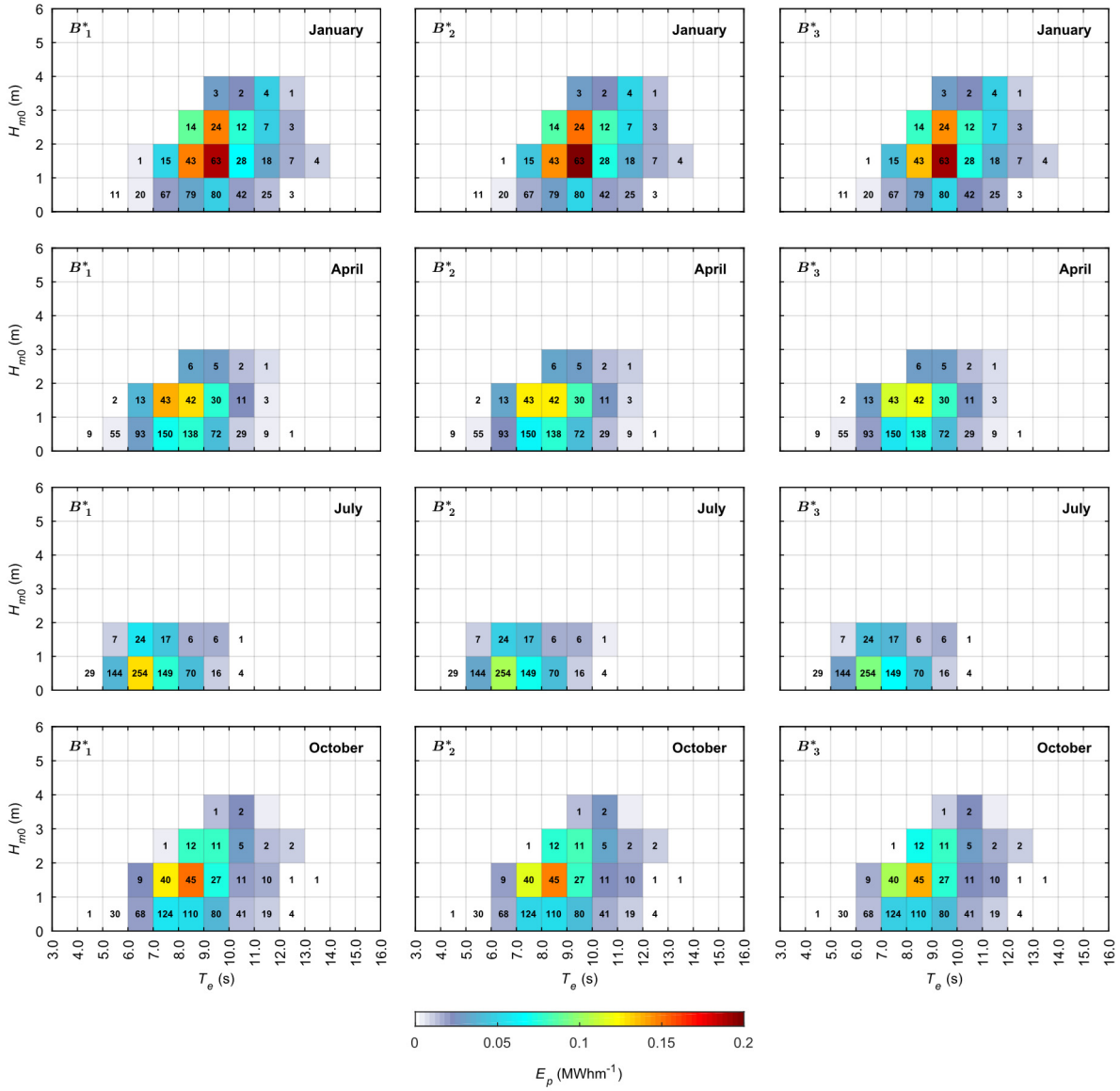


Figure 6. Intra-annual energy capture matrices of the OWC for the three values of the damping coefficient ($B^*_1 = 84.85$; $B^*_2 = 132.18$; $B^*_3 = 160.49$) and four months. The colour scale indicates the total pneumatic energy per unit width of converter absorbed by the device in each energy bin (E_p) and the numbers provide the occurrence, in hours, of the sea states within that bin.

Instead of considering individual energy bins, it may be interesting to analyse the intra-annual variability of the OWC performance for the entire wave climate (Figure 7). Given that, first, there is a great intra-annual variability throughout the year (Figure 5), and second, the captured energy is highly influenced by the available energy [32], the great variability in the intra-annual captured energy (Figure 7) is to be expected. The total annual captured energy changes as a function of the value of the damping coefficient from $E_{w,\,annual} = 8.3$ MWhm^{-1} for B^*_1, to $E_{w,\,annual} = 8.2$ MWhm^{-1} for B^*_2, and $E_{w,\,annual} = 7.8$ MWhm^{-1} for B^*_3. The increase in the captured energy between the least and the most

energetic months is of 230%, 290% and 300% for B^*_1, B^*_2, and B^*_3, respectively, i.e., the lower the value of the damping coefficient, the lower the intra-annual variability in the captured energy, which emphasises again the influence of the turbine-induced damping on the intra-annual variability in the captured energy. Comparing these values with the increase on the available energy between the least and the most energetic months mentioned above, it can be seen that the variability in the intra-annual captured energy is lower than in the intra-annual available energy, for the three values of the turbine-induced damping.

The lower variability shown by the intra-annual captured energy in comparison with that of the intra-annual available energy is related to the configuration of the efficiency matrices, in which sea states with high wave heights and medium to large periods (high-power sea states) present lower values of the capture-width ratio than sea states with low wave heights and periods (low-power sea states). High-power sea states are common in winter months when the available wave energy is higher and low-power sea states are common in summer months when the available energy is lower (Figure 4 and Figure 5), a fact which tends to reduce the variability in the intra-annual captured energy. Here, an interesting point arises: in order to reduce the intra-annual variability in the captured energy, it is necessary to maximise the performance of the device in the months with the lowest resource. Taking into account that, as shown above in Figure 4, the wave energy resource distribution varies throughout the year in such a way that the bulk of energy moves towards lower energy periods and wave heights during summer months, this optimisation process should be conducted when designing the converter for an specific coastal location.

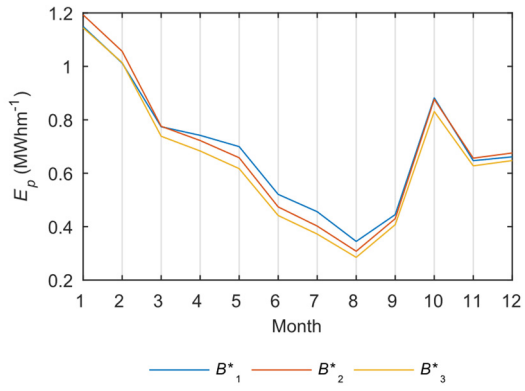


Figure 7. Intra-annual pneumatic energy captured by the OWC in an average year for the three values of the damping coefficient ($B^*_1 = 84.85$; $B^*_2 = 132.18$; $B^*_3 = 160.49$).

The intra-annual capture-width ratio is presented for the three values of the damping coefficient in Figure 8. It can be clearly seen that, as pointed above, the intra-annual capture-width ratio follows

an inverse trend of that of the intra-annual available energy (Figure 5), which reduces the variability in the intra-annual captured energy when comparing with the intra-annual available energy. Therefore, the present OWC converter constitutes a good design for reducing the intra-annual variability in the captured energy. This result applies to the three values of the damping, although with different intensity: the lower the value of the damping coefficient, the higher the intra-annual variability in the capture-width ratio. Furthermore, it can be seen that the value of the damping coefficient that performs best in each month varies throughout the year (Figure 8). In January, February, November and December the intermediate damping (B^*_2) achieves the higher values of the capture-width ratio. From April to September, the lowest damping (B^*_1) performs best. In March and October both values of the damping coefficient, B^*_1 and B^*_2, provide virtually equal values of the capture-width ratio. The highest damping (B^*_3), however, does not provide the best performance in any month, thereby its use is inadvisable at this particular site.

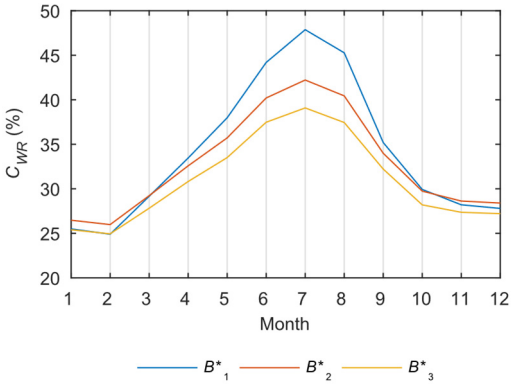


Figure 8. Intra-annual capture-width ratio (C_{WR}) of the OWC in an average year for the three values of the damping coefficient ($B^*_1 = 84.85$; $B^*_2 = 132.18$; $B^*_3 = 160.49$).

As regards the intra-annual captured energy, the turbine-induced damping also plays an important role. In order to appropriately analyse its influence, in Figure 9 the intra-annual variation of the relative difference in the energy captured by the OWC is presented for two values of the damping coefficient. When the OWC is operating with the lowest damping, the captured energy increases throughout the year (with the exception of February) if comparing with the captured energy under the highest damping; the greatest differences are achieved in July with an increase of the captured energy of 18.4%. When comparing the performance of the lowest damping with respect to the intermediate one, there is an increase of the captured energy starting in April with 2.6%, progressively rising up to a maximum of 11.8% in July and, from that point on, progressively reducing again down to 0.6% in

October; in the months of January, February, March, November and December the captured energy decreases in percentages always below 4.3%, with this minimum value being attained in February.

These results add another criterion for selecting the optimum damping for a given study site. In the present case, in which the total annual captured energy is very close for the lowest and intermediate values of the damping coefficient ($E_{w,\,annual}$ = 8.3 MWhm^{-1} and $E_{w,\,annual}$ = 8.2 MWhm^{-1}, respectively), the lower variability in the intra-annual captured energy achieved by the lowest damping (Figure 7) reinforces the selection of the lowest turbine-induced damping as the best performing one. What is more, even in those cases in which the total annual captured energy is slightly greater for a given value of the damping coefficient, it could be interesting to select another damping coefficient if it ensures a greater amount of captured energy in summer months, or what is the same, a lower variability in the intra-annual captured energy. This could be the case of the energy supply on an off-grid system, e.g., an island, in which the provision of energy all over the year is of paramount importance. Is this situation, the converter should be designed in order to minimise the intra-annual variability in the captured energy. The requirement is to supply sufficient energy throughout the year. Thus, the analysis cannot be focused on achieving great annual numbers of captured energy but harnessing enough energy in the months in which the resource is scarce. At this point, knowing the intra-annual electricity demand could shed light on determining the most disadvantageous month.

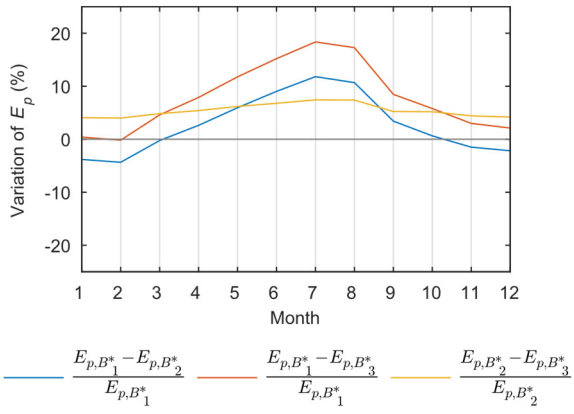


Figure 9. Intra-annual variation of the relative difference between the energy captured by the OWC for two different values of the damping coefficient.

Finally, based on the results achieved, the question arises as to whether the turbine-induced damping could be adapted for matching the optimum damping on a monthly basis, thereby maximising the captured energy. This is not possible with self-rectifying impulse turbines given that

the damping is mainly determined by the turbine diameter (an invariable parameter) and virtually independent of the rotational speed [14]. This impossibility, i.e., the fact that the turbine-induced damping is constant during the entire life of the turbine, makes it all the more important to apply an intra-annual analysis to select the most appropriate value. Moreover, from the point of view of the turbine efficiency, adjusting the rotational speed without modifying the turbine-induced damping is an important benefit, because the turbine rotational speed can be optimised without affecting the hydrodynamic performance of the chamber. A different situation occurs in the case of an OWC equipped with a Wells turbine, whose rotational speed affects the damping exerted on the system [14], enabling the adjustment of the turbine-induced damping depending on the month. However, a careful and complex analysis is necessary given that, when the damping of the turbine changes, the efficiency of the hydrodynamic process of wave energy absorption also changes. This is a topic that deserves further study; however, it is out of the scope of this work, since a different methodology capable of emulating a linear turbine and different values of the damping coefficient must be applied depending on the rotational speed of the turbine.

5. Conclusions

In this work a methodology based on a combination of numerical and physical modelling—thus, considering non-linear effects, and in particular air compressibility—was applied to comprehensively analyse a usually disregarded factor when evaluating the energy production of an OWC wave energy converter at a given coastal site: the intra-annual variability in the performance of the device. To this end, the intra-annual variability in the performance of an OWC wave energy converter was comprehensively analysed through a case study in Galicia (NW Spain). First, numerical modelling was used to characterise, by means of a high-resolution procedure, the intra-annual wave energy resource, which yielded site-specific intra-annual characterisation matrices. Second, physical modelling was used to obtain the three efficiency matrices of the OWC converter (one per each value of turbine-induced damping considered). Finally, the intra-annual energy capture matrices were computed by combining the resource and efficiency matrices.

It was found that the wave energy resource at the study site presents significant intra-annual variability. Between the month with the lowest (July) and the greatest (January) available energy the difference is over 400%. Importantly, not only the amount of available energy varies but also its distribution across sea states: in winter the bulk of energy is provided by sea states with energy

periods in the range 9 s < T_e < 10 s and significant wave heights in the range 1 m < H_{m0} < 3 m; these ranges evolve towards lower energy periods and lower significant wave heights in summer (6 s < T_e < 7 s, and 0 m < H_{m0} < 1 m, respectively). As both parameters (energy period and significant wave height) greatly influence the capture-width ratio of the OWC, it follows that a high-resolution intra-annual wave energy characterisation is fundamental to correctly characterise the performance of an OWC throughout the year.

Regarding the intra-annual variability in the energy captured, the following conclusions may be drawn. First, the intra-annual captured energy follows the same trend as the intra-annual available energy. However, the variability in the intra-annual captured energy is slightly weaker thanks to the design of the OWC, that exhibits a better performance when the available energy is lower, that is, in summer months—characterised by lower energy periods and smaller significant wave heights, for which the capture-width ratios are higher. Second, the intra-annual variability in the captured energy changes its intensity depending on the damping coefficient, which adds another criterion for selecting the optimum damping for a given study site. In the study case, the lower the value of the damping coefficient, the lower the variability in the captured energy. Finally, it was found that the turbine-induced damping which maximises the energy capture of the OWC is not constant, and depends on the succession of sea states in the period considered for the maximisation; in the study case, considering monthly periods, the optimum value varied from one month to the next. Taking the entire year as the period for the maximisation of the energy capture, the lowest value of the damping coefficient (B^*_1 = 84.85) was found to be the best of those considered, for it provided the largest annual captured energy along with the lowest intra-annual variability.

In sum, the turbine-induced damping ought to be regarded as one of the fundamental elements when designing an OWC plant, as it significantly affects the energy capture. However, an inter-annual analysis is not enough, given that the damping that maximises the performance of the OWC changes on a monthly basis. Therefore, to select the most appropriate turbine-induced damping overall—that is, for dimensioning the turbine—for a given site of interest both the turbine-induced damping and a high-resolution characterisation of the wave energy resource, carried out at an intra-annual level, are in order.

Acknowledgements

During this work I. López was supported by the postdoctoral grant ED481D 2019/019 of the 'Programa de Axudas á etapa posdoutoral da Xunta de Galicia (Consellería de Educación, Universidade e Formación Profesional)'.

References

[1] López M, Veigas M, Iglesias G. On the wave energy resource of Peru. Energy Conv Manag 2015;90:34-40. https://dx.doi.org/10.1016/j.enconman.2014.11.012

[2] Weiss CVC, Guanche R, Ondiviela B, Castellanos OF, Juanes J. Marine renewable energy potential: A global perspective for offshore wind and wave exploitation. Energy Conv Manag 2018;177:43-54. https://doi.org/10.1016/j.enconman.2018.09.059

[3] O'Dea A, Haller MC, Özkan-Haller HT. The impact of wave energy converter arrays on wave-induced forcing in the surf zone. Ocean Eng 2018;161:322-36. https://doi.org/10.1016/j.oceaneng.2018.03.077

[4] Perez J, Menendez M, Losada IJ. GOW2: A global wave hindcast for coastal applications. Coast Eng 2017;124:1-11. https://doi.org/10.1016/j.coastaleng.2017.03.005

[5] Lavidas G, Venugopal V. A 35 year high-resolution wave atlas for nearshore energy production and economics at the Aegean Sea. Renew Energy 2017;103:401-17. https://doi.org/10.1016/j.renene.2016.11.055

[6] Zheng S, Zhang Y, Iglesias G. Coast/breakwater-integrated OWC: A theoretical model. Mar Struct 2019;66:121-35. https://doi.org/10.1016/j.marstruc.2019.04.001

[7] Perez-Collazo C, Pemberton R, Greaves D, Iglesias G. Monopile-mounted wave energy converter for a hybrid wind-wave system. Energy Conv Manag 2019;199:111971. https://doi.org/10.1016/j.enconman.2019.111971

[8] Ramos V, López M, Taveira-Pinto F, Rosa-Santos P. Influence of the wave climate seasonality on the performance of a wave energy converter: A case study. Energy 2017;135:303-16. https://doi.org/10.1016/j.energy.2017.06.080

[9] Carballo R, Sánchez M, Ramos V, Fraguela JA, Iglesias G. Intra-annual wave resource characterization for energy exploitation: A new decision-aid tool. Energy Conv Manag 2015;93:1-8. https://doi.org/10.1016/j.enconman.2014.12.068

[10] Carballo R, Iglesias G. A methodology to determine the power performance of wave energy converters at a particular coastal location. Energy Conv Manag 2012;61:8-18. https://dx.doi.org/10.1016/j.enconman.2012.03.008

[11] Neill SP, Hashemi MR. Wave power variability over the northwest European shelf seas. Appl Energy 2013;106:31-46. https://dx.doi.org/10.1016/j.apenergy.2013.01.026

[12] Carballo R, Sánchez M, Ramos V, Fraguela JA, Iglesias G. The intra-annual variability in the performance of wave energy converters: A comparative study in N Galicia (Spain). Energy 2015;82:138-46. https://doi.org/10.1016/j.energy.2015.01.020

[13] Guillou N, Chapalain G. Annual and seasonal variabilities in the performances of wave energy converters. Energy 2018;165:812-23. https://doi.org/10.1016/j.energy.2018.10.001

[14] Falcão AFO, Henriques JCC. Oscillating-water-column wave energy converters and air turbines: A review. Renew Energy 2016;85:1391-424. https://dx.doi.org/10.1016/j.renene.2015.07.086

[15] Chen F, Duan D, Han Q, Yang X, Zhao F. Study on force and wave energy conversion efficiency of buoys in low wave energy density seas. Energy Conv Manag 2019;182:191-200. https://doi.org/10.1016/j.enconman.2018.12.074

[16] Oliveira P, Taveira-Pinto F, Morais T, Rosa-Santos P. Experimental evaluation of the effect of wave focusing walls on the performance of the Sea-wave Slot-cone Generator. Energy Conv Manag 2016;110:165-75. https://doi.org/10.1016/j.enconman.2015.11.071

[17] Falcão AFO, Henriques JCC, Gato LMC. Self-rectifying air turbines for wave energy conversion: A comparative analysis. Renew Sust Energ Rev 2018;91:1231-41. https://doi.org/10.1016/j.rser.2018.04.019

[18] Strati FM, Malara G, Arena F. Performance optimization of a U-Oscillating-Water-Column wave energy harvester. Renew Energy 2016;99:1019-28. https://doi.org/10.1016/j.renene.2016.07.080

[19] Zheng S, Antonini A, Zhang Y, Greaves D, Miles J, Iglesias G. Wave power extraction from multiple oscillating water columns along a straight coast. J Fluid Mech 2019;878:445-80. http://dx.doi.org/10.1017/jfm.2019.656

[20] Falcão AFO, Rodrigues RJA. Stochastic modelling of OWC wave power plant performance. Appl Ocean Res 2002;24:59-71. https://doi.org/10.1016/S0141-1187(02)00022-6

[21] Falcão AFO. Stochastic modelling in wave power-equipment optimization: maximum energy production versus maximum profit. Ocean Eng 2004;31:1407-21. http://dx.doi.org/10.1016/j.oceaneng.2004.03.004

[22] Gomes RPF, Henriques JCC, Gato LMC, Falcão AFO. Hydrodynamic optimization of an axisymmetric floating oscillating water column for wave energy conversion. Renew Energy 2012;44:328-39. https://doi.org/10.1016/j.renene.2012.01.105

[23] Sheng W. Power performance of BBDB OWC wave energy converters. Renew Energy 2019;132:709-22. https://doi.org/10.1016/j.renene.2018.07.111

[24] Bailey H, Robertson BRD, Buckham BJ. Wave-to-wire simulation of a floating oscillating water column wave energy converter. Ocean Eng 2016;125:248-60. https://doi.org/10.1016/j.oceaneng.2016.08.017

[25] Henriques JCC, Portillo JCC, Sheng W, Gato LMC, Falcão AFO. Dynamics and control of air turbines in oscillating-water-column wave energy converters: Analyses and case study. Renew Sust Energ Rev 2019;112:571-89. https://doi.org/10.1016/j.rser.2019.05.010

[26] Falcão AFO, Gato LMC, Nunes, E P A S. A novel radial self-rectifying air turbine for use in wave energy converters. Renew Energy 2013;50:289-98. https://doi.org/10.1016/j.renene.2012.06.050

539 [27] Faÿ F, Robles E, Marcos M, Aldaiturriaga E, Camacho EF. Sea trial results of a predictive
540 algorithm at the Mutriku Wave power plant and controllers assessment based on a detailed plant
541 model. Renew Energy 2020;146:1725-45. https://doi.org/10.1016/j.renene.2019.07.129

542 [28] Benreguig P, Kelly J, Pakrashi V, Murphy J. Wave-to-Wire Model Development and Validation
543 for Two OWC Type Wave Energy Converters. Energies 2019;12
544 https://doi.org/10.3390/en12203977

545 [29] Hirt CW, Nichols BD. Volume of fluid (VOF) method for the dynamics of free boundaries. J
546 Comput Phys 1981;39:201-25. http://doi.org/10.1016/0021-9991(81)90145-5

547 [30] López I, Pereiras B, Castro F, Iglesias G. Holistic performance analysis and turbine-induced
548 damping for an OWC wave energy converter. Renew Energy 2016;85:1155-63.
549 https://dx.doi.org/10.1016/j.renene.2015.07.075

550 [31] Lisboa RC, Teixeira PRF, Torres FR, Didier E. Numerical evaluation of the power output of an
551 oscillating water column wave energy converter installed in the southern Brazilian coast. Energy
552 2018;162:1115-24. https://doi.org/10.1016/j.energy.2018.08.079

553 [32] López I, Carballo R, Iglesias G. Site-specific wave energy conversion performance of an
554 oscillating water column device. Energy Conv Manag 2019;195:457-65.
555 https://doi.org/10.1016/j.enconman.2019.05.030

556 [33] López I, Pereiras B, Castro F, Iglesias G. Performance of OWC wave energy converters:
557 influence of turbine damping and tidal variability. Int J Energy Res 2015;39:472-83.
558 https://doi.org/10.1002/er.3239

559 [34] López I, Castro A, Iglesias G. Hydrodynamic performance of an oscillating water column wave
560 energy converter by means of particle imaging velocimetry. Energy 2015;83:89-103.
561 http://dx.doi.org/10.1016/j.energy.2015.01.119

562 [35] López I, Pereiras B, Castro F, Iglesias G. Optimisation of turbine-induced damping for an OWC
563 wave energy converter using a RANS–VOF numerical model. Appl Energy 2014;127:105-14.
564 https://doi.org/10.1016/j.apenergy.2014.04.020

565 [36] Iglesias G, Carballo R. Wave energy potential along the Death Coast (Spain). Energy
566 2009;34:1963-75. https://doi.org/10.1016/j.energy.2009.08.004

567 [37] Carballo R, Arean N, Álvarez M, López I, Castro A, López M et al. Wave farm planning through
568 high-resolution resource and performance characterization. Renew Energy 2019;135:1097-107.
569 https://doi.org/10.1016/j.renene.2018.12.081

570 [38] Chakrabarti SK. Offshore structure modeling. Singapore: World Scientific, 1994

571 [39] López I, Carballo R, Taveira-Pinto F, Iglesias G. Sensitivity of OWC performance to air
572 compressibility. Renew Energy 2020;145:1334-47. https://doi.org/10.1016/j.renene.2019.06.076

573 [40] Simonetti I, Cappietti L, Elsafti H, Oumeraci H. Evaluation of air compressibility effects on the
574 performance of fixed OWC wave energy converters using CFD modelling. Renew Energy
575 2018;119:741-53. https://doi.org/10.1016/j.renene.2017.12.027

576 [41] Falcão AFO, Henriques JCC. Model-prototype similarity of oscillating-water-column wave
577 energy converters. Int J Mar Energy 2014;6:18-34.
578 https://dx.doi.org/10.1016/j.ijome.2014.05.002

579 [42] Falcão AFO, Gato LMC. 8.05 - Air Turbines. In: Sayigh A, editor. Comprehensive Renewable
580 Energy, Oxford: Elsevier; 2012, p. 111-149. https://dx.doi.org/10.1016/B978-0-08-087872-
581 0.00805-2

582 [43] Elhanafi A, Macfarlane G, Fleming A, Leong Z. Experimental and numerical investigations on
583 the hydrodynamic performance of a floating–moored oscillating water column wave energy
584 converter. Appl Energy 2017;205:369-90. https://doi.org/10.1016/j.apenergy.2017.07.138

585 [44] Perez-Collazo C, Greaves D, Iglesias G. Hydrodynamic response of the WEC sub-system of a
586 novel hybrid wind-wave energy converter. Energy Conv Manag
587 2018;171:307-25. https://doi.org/10.1016/j.enconman.2018.05.090

588 [45] Hasselmann DE, Dunckel M, Ewing JA. Directional wave spectra observed during JONSWAP
589 1973. J Phys Oceanogr 1980;10:1264-80. https://doi.org/10.1175/1520-0485(1980)010<
590 1264:DWSODJ>2.0.CO;2

591